ORIGINAL PAPER

Representativeness of the particulate matter pollution assessed by an official monitoring station of air quality in Santiago, Chile: projection to human health

Margarita Préndez [ID] · **Patricio Nova** [ID] ·
Hugo Romero [ID] · **Flávio Mendes** [ID] ·
Raúl Fuentealba [ID]

Abstract Santiago, capital city of Chile, presents air pollution problems for decades mainly by particulate matter, which significantly affects population health, despite national authority efforts to improve air quality. Different properties of the particulate matter (PM_{10}, $PM_{2.5}$ and PM_1 fractions, particle surface and number) were measured with an optical spectrometer. The sampling was done during spring 2019 at different sites within the official representative area of Independencia monitoring station (ORMS-IS). The results of this study evidence large variations in PM mass concentration at small-scale areas within the ORMS-IS representative zone, which reports the same value for the total area. Results from PM properties such as PM_1, particle number and particle surface distribution show that these properties should be incorporated in regular monitoring in order to improve the understanding of the effects of these factors on human health. The use of urban-climate canopy-layer models in a portion of the sampled area around the monitoring station demonstrates the influence of street geometry, building densities and vegetation covers on wind velocity and direction. These factors, consequently, have an effect on the potential for air pollutants concentrations. The results of this study evidence the existence of hot spots of PM pollution within the area of representativeness of the ORMS-IS. This result is relevant from the point of view of human health and contributes to improve the effectiveness of emission reduction policies.

M. Préndez (✉) · P. Nova · R. Fuentealba
Facultad de Ciencias Químicas y Farmacéuticas, Laboratorio de Química de la Atmósfera y Radioquímica, Sergio Livingstone 1007, Independencia, Universidad de Chile, 8380492 Santiago, Chile
e-mail: mprendez@ciq.uchile.cl

H. Romero
Facultad de Arquitectura y Urbanismo, Laboratorio de Medio Ambiente y Territorio, Universidad de Chile, 8320000 Santiago, Chile

F. Mendes
Escuela Superior de Agricultura "Luiz de Queiroz", Doutorando Em Ciências Florestais, Universidade de Sao Paulo, Piracicaba, Brasil

Introduction

For decades, Santiago de Chile has been affected by high levels of atmospheric pollution. The outstanding pollutant is the atmospheric aerosol, also called particulate matter (PM), which has relevant effects, on the environment and on human health (Jorquera,

2020). The Health Effects Institute (HEI, 2019) estimates that air pollution (PM$_{2.5}$ and ozone) is the fifth risk factor for mortality worldwide, and in 2017, it was estimated that air pollution contributed to about 5 million deaths worldwide representing almost 10% of total fatalities. Over 55% of the world's population live in urban areas and this is set to rise to 68% by 2050 (WHO, 2022.

Variability of PM concentrations depends on different factors including local emissions, atmospheric conditions and urban morphology (Buccolieri et al., 2010; Hofman et al., 2013), causing significant spatial and temporal differences in air quality in relatively small areas. Current monitoring network distribution and its expected spatial resolution do not necessarily capture PM variability (Karner et al., 2010; Zikova et al., 2017). Official Representative Monitoring Stations (ORMSs) installed in Chile have a spatial resolution of 2 km radius. However, the official criteria are the population size within these two kilometres, location and sampling conditions (MINSAL, 1998; MMA, 2017). These criteria ignore spatial and temporal pollutants heterogeneity, the distance from the sources and magnitude, the variability of local ventilation and the complexity of urban morphology, contravening the objective of monitoring to determine population daily exposure to pollutants. Inadequate monitoring spatial resolution difficult the estimation of individual exposure to PM, hence offering insufficient information for epidemiological studies of pollutants effects on health; it also does not provide an understanding of the effectiveness of emission reduction policies (Kelly et al., 2017; Tsai et al., 2019), therefore having negative implications for an adequate environmental management.

The National Air Quality Information System (SINCA for its acronym in Spanish) of the Chilean Environmental Ministry (Ministerio del Medio Ambiente, MMA) registers air quality in the country, and it is constantly seeking to improve its monitoring and data management capabilities. In the Metropolitan Region (RM), in which Santiago city is located, the air quality monitoring network known as MACAM-RM has eleven stations (Fig. 1) for continuous particulate matter (PM$_{2.5}$ and PM$_{10}$), and gases (SO$_2$, NOx, CO, O$_3$ and non-methane hydrocarbons (HCNM)) measurements.

The MACAM-RM monitoring network uses two types of continuous PM measurement instruments

according to national regulations (DS N°59/1998 and DS N°12/2011): Oscillating Conical Element Microbalance (TEOM) and Beta attenuation monitors (BAM). These instruments are expensive with costly operation and maintenance, which limits the possibility of studying the spatial distribution of PM data (Kelly et al., 2017; Wang et al., 2015). The recent availability of instruments based on optical principles of indirect measurement is an interesting alternative to the more expensive instruments used by the MACAM-RM network (Grimm & Eatough, 2009; Holstius et al., 2014; Kelly et al., 2017; Kumar et al., 2015). These alternative instruments are portable and easy to use, which increases the ability to improve PM characterization with high spatio-temporal resolution at a lower cost.

The Metropolitan area of Santiago is divided in 52 municipalities, 34 located in the urban area (or Grand Santiago, henceforth Santiago), and 18 located in rural areas. This study focuses in the urban municipalities (Fig. 1). Besides climatological differences in wind, humidity and temperature (e.g. presence of heat islands) among the municipalities, there is also a marked socio-economical differentiation between the richest areas located to the NE and the rest of the city, where middle- and low-income classes are dominant (Sarricolea et al., 2022).

Hitherto, relevant properties of atmospheric aerosol that have negative impacts on human health, especially in polluted areas, such as highly populated cities, is neither fully investigated nor well understood (Bind et al., 2012; Kuuluvainen et al., 2016; Tsai et al., 2019). Particle number has been associated with adverse health effects such as respiratory diseases among children in urban areas (Li et al., 2016), effects on fibrinogen, i.e. a type of tumour marker (Bind et al., 2012), and in inflammatory markers (Tsai et al., 2019). Systematic studies and meta-analyses (Dinoi et al., 2017; Forlivesi et al., 2018) of the effects of exposure to PM on health have found associations with morbidity and mortality in the population. The above examples complemented with adequate techniques for elemental analysis can be useful to improve physical and chemical characterization of PM (Galvão et al., 2018) and to identify stationary sources that affect a determined area (Fuentealba, 2018; Leoni et al., 2018; Préndez et al., 2007).

Particle surface distribution is emerging as a useful PM property to investigate health effects due to
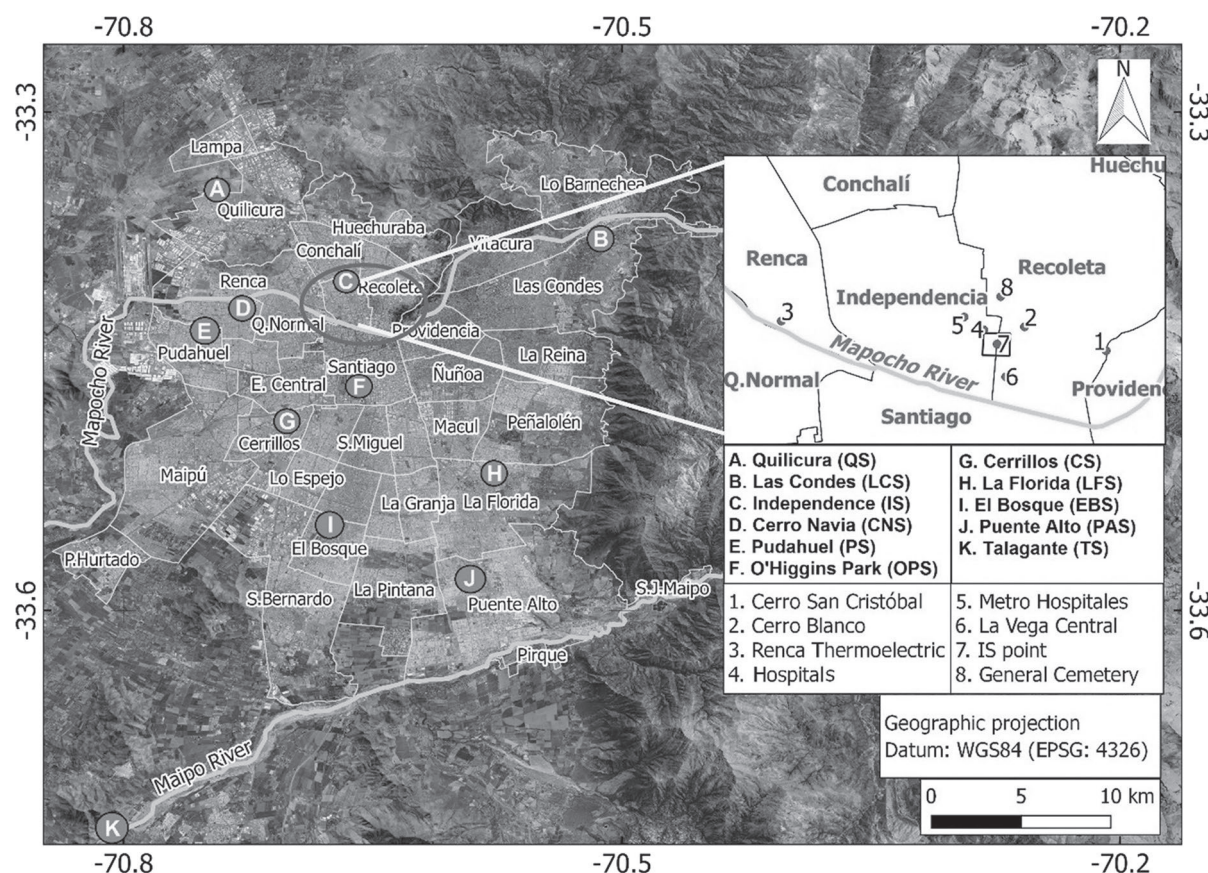
Fig. 1 Grand Santiago (grey area), its municipalities (light grey delimitations), and main geographical features around the sampling area (zoomed in box): San Cristobal and Blanco hills, Mapocho River, open market (La Vega) and public services (hospitals, underground subway station, thermoelectric plant and cemeteries) marked with 1–8 numbers, and MACAM-RM network monitoring stations indicated with A–K letters

exposure to PM (Kuuluvainen et al., 2016; Ntziachristos et al., 2007). A larger particle surface area could increase the kinetic and thermodynamic potential of chemical reactions in the atmosphere, which can exacerbate pollution. This property is an indication of the internal structure of the particle, such as porosity, that increase particle surface, potentially retaining other pollutants (Cassee et al., 2013; Long et al., 2013; Guo et al., 2017) or even viruses such as SARS-2 (Setti et al., 2020; Zoran et al., 2020), within the particle.

In addition, the monitoring of particle surface distribution contributes to the assessment of pollution reduction policies. Reduction of a 67.2% and 65.0% in particle number concentration and particle surface area has been reported between days with and without vehicle restriction, respectively (Zhao & Yu, 2017). The effect of vehicle circulation restriction on air pollution near a sampling location depends on the distance between the relative orientation of the sampling site and the traffic-restricted areas, as well as on meteorological conditions (Zhao & Yu, 2017).

This study evaluates if an ORMS has the capability to capture i) spatial heterogeneity in PM measurements and ii) urban characteristics of various sampling sites within the station representative area, using a portable visible spectrophotometer to measure PM properties that are not currently quantified by the national monitoring authority.

Materials and methods

Study area

The Metropolitan Region of Santiago is located within the basin conformed by Maipo and Mapocho river valleys that descend from the Andes Cordillera, and concentrates about 40% of the country's population (19 828 563 inhabitants, projection to 30 June 2022, INE, 2022). West of Santiago, the basin is constrained by a coastal mountain range that separates the city from the Pacific Ocean by approximately 130 km. Transversal hills join both mountain ranges substantially reducing atmospheric ventilation at the basin. Since the city is located at a subtropical latitude (33°S), the Mediterranean type of regional climate is under the prevalence of anticyclone influences, and a marked seasonal temperature and rainfall variation, with warm and dry summers and cool and wet winters. Climate at the region, however, has shown a tendency to drier conditions over the last decade due to the ongoing mega-drought that affects central Chile The presence of a persistent radiative thermal inversion layer above the basin explain the remarkable stable atmospheric conditions present over Santiago during the year, which intensify during the winter months. (DMC, 2021). In addition to a large city population, Santiago concentrates most of the country's industries and services, representing more than 50% of the national Gross Domestic Product (GDP).

The air pollution monitoring station used in this work is located in the Independencia municipality that has around 100 000 inhabitants, positioned in the middle rank of the human development and social indicators (Romero et al., 2010). The monitoring station (ORMS-IS) is part of the MACAM-RM monitoring network. The station is representative of an area that includes parts of Independencia, Recoleta and Santiago municipalities. It is located north of the historical centre of Santiago city and includes many important urban features, for instance, the Mapocho River, the main metropolitan park and zoo (San Cristóbal hill), the largest open market (La Vega) and large cemeteries. Two high traffic roads (Independencia and La Paz avenues) cross the area from north to south and another one (Santa Maria Avenue) from west to east. These avenues connect other municipalities with the city centre and also allow access to several large services such as hospitals, a university campus and an underground subway station. In addition, a thermoelectric plant is located about 1.5 km west of Independencia. During recent years, the predominant middle-class one-story houses have been replaced by tall apartment buildings occupied both by national and migrant population (Fig. 1).

The selected sampling sites in this study locate within a radius of 2 km (Fig. 2) from the ORMS-IS and have the purpose to characterize a population area similar to the area represented by the ORMS-IS.

Sampling and characteristics of the sampled sites

Sampling was performed during two weeks between 4 and 6 September, and between 10 and 12 September 2019. This month of the year corresponds to the period that follows the critical PM pollution episodes that occur during the austral autumn–winter months (April–August). These episodes relate to various factors that generate low atmospheric PM dispersion (Préndez et al., 2011; Toro et al., 2014). Figure 2 shows the 15 sampling sites reported in this study, labelled according to cardinal direction and distance from the ORMS-IS.

Sampling was performed by a GRIMM spectrometer, Mini-LAS 11-E model with GRIMM Spectrometer 1158-EE Sensor, located 1.75 m above ground level according to the protocol for population exposure to urban pollution (USEPA, 2004). A time resolution of 1 min was used for two periods of 30 min to measure PM_{10}, $PM_{2.5}$ and PM_1 fractions during one period, and the surface distribution and the particle number during the other. The spectrometer has a laser diode with a wavelength in the visible range of 660 nm. The intensity of the laser beam is modulated to detect particles between 0.25 μm and 32 μm and classify them into 31 channels within the range (Grimm & Eatough, 2009).

Vehicle traffic of the study area was obtained using Google Traffic to determine the typical condition or real-time condition in each sampling area. The system detects traffic information, non-moving vehicles, road accidents, and road constructions, using GPS signals of smartphones within each car on the streets. Subsequently, the sampling sites were classified according to vehicle traffic, as shown in Table 1.
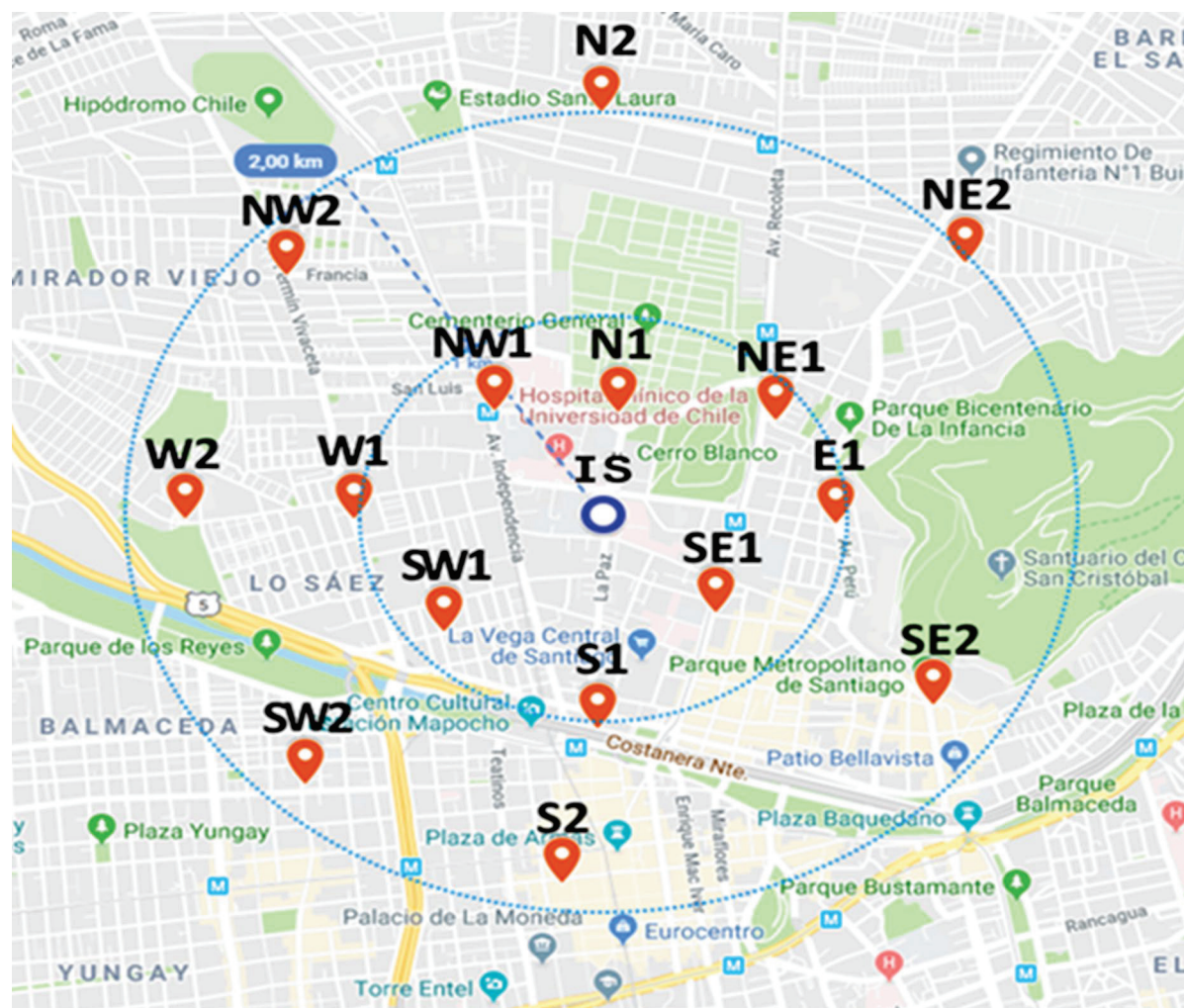
Fig. 2 Sampling sites within the representative area of the ORMS-IS

Table 1 Level of the traffic at each sampling site within the representative area of ORMS-IS. Source: Google Traffic

High traffic	Indicates slow traffic in the sector due to the large number of vehicles circulating at that moment
Medium traffic	Indicates an intermediate level of traffic in the sector
Medium/low traffic	Indicates that sectors with medium and low traffic were observed near the sampling site
Low traffic	Indicates a low level of traffic in the sector and an expeditious travel speed

Statistics and data

PM_{10}, $PM_{2.5}$ and PM_1 mass concentrations were analysed using Box Plots obtained from the "R" statistical software. Particle number and particle surface distribution were obtained using the Spectrometer_V7-1 Software provided by the Grimm spectrometer and plotted using Excel.

Temperature and relative humidity (RH) were measured using an 1158-EE sensor from the Grimm spectrometer. The temperature effect on the spectrometer's performance is negligible in the range from

5 °C to 32 °C (Holstius et al., 2014; Zikova et al., 2017). High levels of RH affect the light scattering principle of measurement due to PM absorbing water vapour, therefore changing the dispersion and absorption coefficients (Dinoi et al., 2017). Wind speed and wind direction were obtained from the MMA, (2019) for each sampling day. Figure 3 shows the wind speed and wind direction at 4–5 m height. Wind data were processed using the Open Air extension of the "R" software.

The lognormal function is the most widely used fit to plot PM mass, size and surface distribution because it gives better adjustments for experimental results, being especially useful for the number of

particle size ranges greater than 10 units (TSI, 2012). Particle number distribution and particle surface distribution (dN/dlogD) were calculated for the 15 sampling sites during the two sampling periods. *X*-axis and *y*-axis are in logarithmic (base 10) scale (details can be found in the SI.

Land use and cover, and urban morphology

Land use and cover, and the urban morphology around the ORMS-IS were analysed using the ENVI-met model (Mendes et al., 2020). This model considers the spatial distribution of streets, houses and buildings, according to type, position, height,
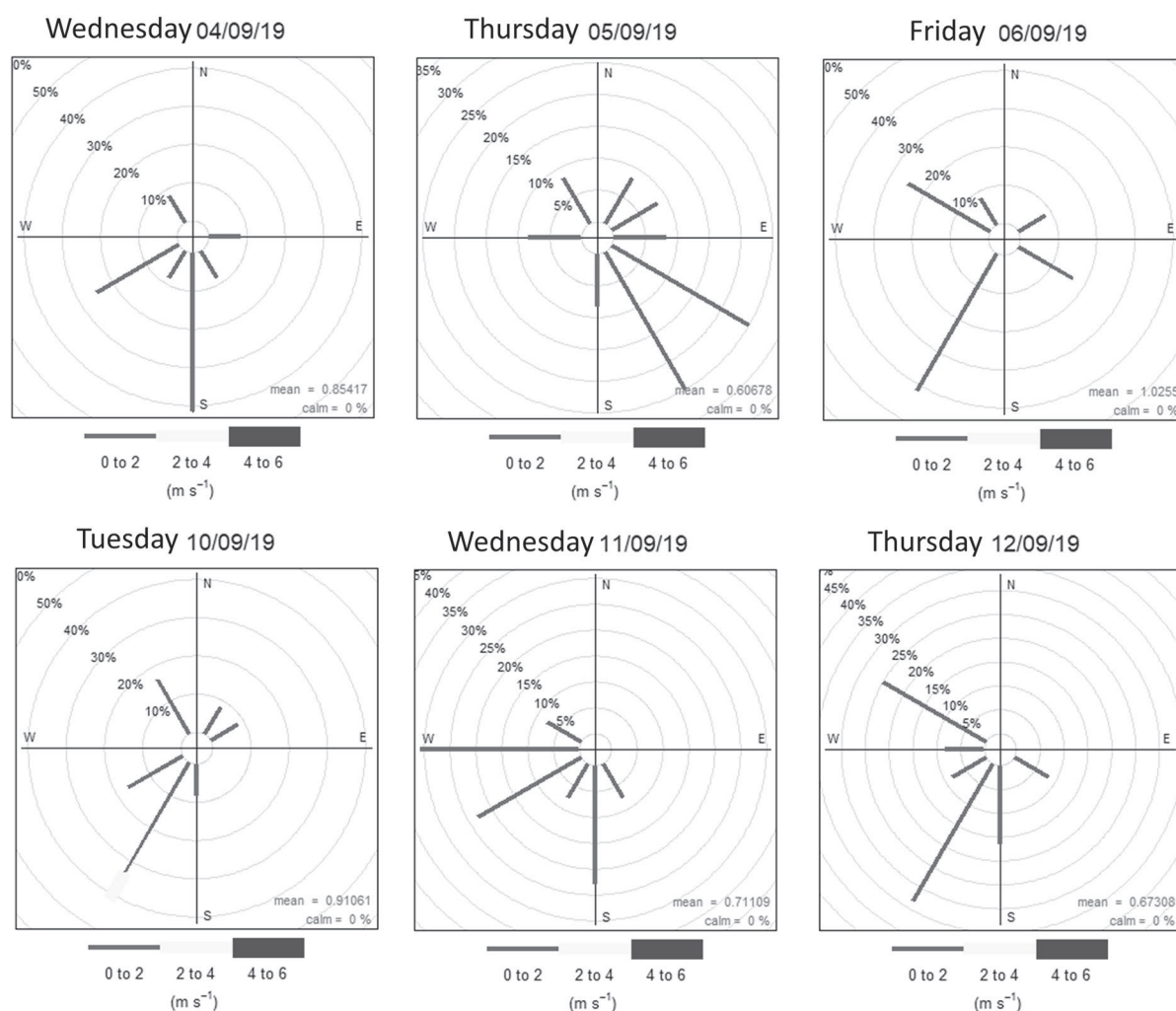
Fig. 3 Wind roses according to frequency (%) and wind speed (m s^{-1}) during the daytime period 4–6 September and 10–12 September 2019 from 7:00 a.m. to 7:00 p.m. local time

and vegetation cover and density obtained from 2015 Google Street View images. The tallest building in the sampling area reaches 20 floors (~60 m height) at Santos Dumont Street near Blanco Hill, but most of the buildings have only one or two floors (between 5 and 6 m height). Vegetation corresponds to palms of 15 m height and lower canopy density (i.e. trees ~10 m height), such as *Robinia pseudoacacia*, *Liquidambar styraciflua*, and *Prunus cerasifera*, dense shrubs (~6 m height), and grass. Predominant land cover corresponds to sand, followed by asphalt, concrete, and water. The modelled selected area, limited by computational restrictions, corresponds to 400×400 m and is located within a 2 km radius from the ORMS-IS (Fig. 2). Figure 4 shows an aerial view of the area (from Google Earth).

Results

Table 2 shows the main characteristics of the sampling sites.

The 15 sampling sites were classified according to typical traffic conditions and sampling time (Table 1). There are two sites with high traffic, two sites with medium traffic, nine sites with medium/low traffic,

and two sites with a low level of traffic. It is probable that different levels of traffic at each site contribute to pollutant concentration heterogeneity within the representative area of the ORMS-IS. During the sampling period, temperature ranged from 14.4 ± 0.3 °C to 26.7 ± 2.1 °C, and relative humidity ranged from $31.6\% \pm 0.7\%$ to $76.0\% \pm 1.8\%$. During the sampling period, only one day (10 September) presented a significant amount of rainfall. Wind speed ranged between 0.2 m s^{-1} and 2.3 m s^{-1}, with SW, S and W as predominant wind directions.

PM_{10}, $PM_{2.5}$ and PM_1 mass concentration

Figure 5 (a, b, and c) shows mass concentration of PM_{10}, $PM_{2.5}$ and PM_1. It can be noted that 11 of the 15 sampled sites present outliers. These outliers can be interpreted as high concentrations in time (single data points) due to the high temporal resolution (1 min) of the spectrometric technique employed.

Figure 5a and 5b shows that the highest concentrations of PM_{10} and $PM_{2.5}$ correspond to 6 September at site NW1, with 339 ± 214 μg m^{-3} and 70 ± 13 μg m^{-3}, respectively. The minimum concentrations of PM_{10} and $PM_{2.5}$ occurred in 11 September at SW2, with 39 ± 7 μg m^{-3} (almost 9 times lower

Fig. 4 Aerial view and modelled land use and cover at the Independencia municipality (location of the ORMS-IS). Building blocks (grey) cover 33% of the surface, bare land (white) 47.6%, trees (dark green) 15.8%, and grass (light green) 3.3%, respectively

Table 2 Sites sampled description of the local sources and the environment within the representative area of the ORMS-IS between 4 and 12 September 2019

Sites	Traffic	t (°C)	RH (%)	Local sources	Green areas
E1	Mid	22.2 ± 0.1	41.6 ± 0.9	no observation	Cerro San Cristóbal (~ 400 m). Trees on the streets, approximately 3 m near the site
SE1	Mid	22.1 ± 0.6	46.5 ± 0.5	High pedestrian flow (Near a College)	Trees on the streets, approximately 15 m near the site
NE1	Mid/low	15.1 ± 0.4	76.0 ± 1.8	Gas station (~ 30 m). La Recoleta Cinerario (~ 500 m)	Cerro Blanco (~ 70 m) -Cerro San Cristóbal (~ 650 m) Located in a square, approximately 10 m near the site
SW1	Mid/low	15.1 ± 0.3	67.3 ± 1.1	Motor vehicles repair (~ 20 m)	Los Reyes Park (~ 700 m)
NW1	High	14.4 ± 0.3	74.2 ± 0.8	High pedestrian flow (metro entrance). Building (~ 70 m). Cinerario of the General Cemetery (~ 700 m)	no observation
W1	Mid/low	18.9 ± 0.7	59.9 ± 1.5	La Estampa Mill (~ 500 m). Three gas station (~ 150 m / ~ 150 m / ~ 60 m)	Trees on the streets, approximately 10 m near the site
N1	Mid/low	15.8 ± 0.3	68.4 ± 1.0	Building (~ 450 m). Cinerario of the General Cemetery (~ 600 m)	Cerro Blanco (~ 300 m) Trees on the streets, approximately 10 m near the site
S1	Mid/low	15.5 ± 0.4	66.5 ± 2.2	La Vega Market (~ 150 m). Street cooking (~ 100 m)	Río Mapocho Slope (~ 30 m) Trees on the streets, approximately 5 m near the site
SE2	Mid/low	20.4 ± 1.1	54.1 ± 3.0	no observation	Entrance fee of Parque Metropolitano Park (~ 20 m)
SW2	Mid/low	20.6 ± 1.3	50.3 ± 3.5	Gas station (~ 50 m)	Located in a square, approximately 20 m near the site. Los Reyes Park(~ 400 m)
S2	High	15.5 ± 0.4	63.3 ± 1.7	High pedestrian flow (Pedestrian walk)	no observation
N2	Low	26.7 ± 2.1	31.6 ± 0.7	Automotive workshop (~ 50 m)	Trees on the streets, approximately 2 m near the site
W2	Low	16.5 ± 0.7	59.6 ± 1.5	Closest site to Renca thermoelectric power plant (~ 1.7 km). Pharmaceutical industry (~ 700 m)	Enel Stadium (~ 100 m). Los Reyes Park (~ 400 m). Located in a square, approximately 20 m near the site
NE2	Mid/low	26.2 ± 1.2	33.8 ± 0.8	no observation	Trees on the streets, approximately 7 m near the site
NW2	Mid/low	24.6 ± 2.6	42.9 ± 3.4	Pharmaceutical industry (~ 600 m)	Trees on the streets, approximately 5 m near the site

than the maximum) for PM_{10}, and 14 ± 2 µg m^{-3} for $PM_{2.5}$. Site SW2 is located at a vegetated area, which could explain the minimum values obtained on 10 and 11 September. A rainfall event occurred in the early morning of the 10 September.

Additional high concentration of $PM_{2.5}$ occurred at site W2 sampled on 12 September, with (131 ± 16) µg m^{-3} and (48 ± 3) µg m^{-3} for PM_{10} and $PM_{2.5}$, respectively. The W2 site is the closest site from the highway Autopista Central and the Renca thermoelectric power plant (see Fig. 1). On 12 September, NW winds were registered. Three other sites sampled on 4 September show similar

levels of $PM_{2.5}$ (29 µg m^{-3} to 33 µg m^{-3}). Concentrations of $PM_{2.5}$ on the other sampling days show higher variation depending on location, with a greater spatial variability at the area of representativeness of the ORMS-IS. Figure 5c shows that the W2 site registered the highest concentration of PM_1, with (36 ± 2) µg m^{-3}, followed by NW1, the site with greatest mass concentrations of PM_{10} and $PM_{2.5}$ (Figs. 5a and 5b). PM_1 and $PM_{2.5}$ have similar sources associated with fossil fuel combustion. The NE2 site, located in a residential sector with no other recorded sources than a medium/low level of vehicular traffic, shows the lowest concentration for PM_1, with (8 ± 2) µg m^{-3}.
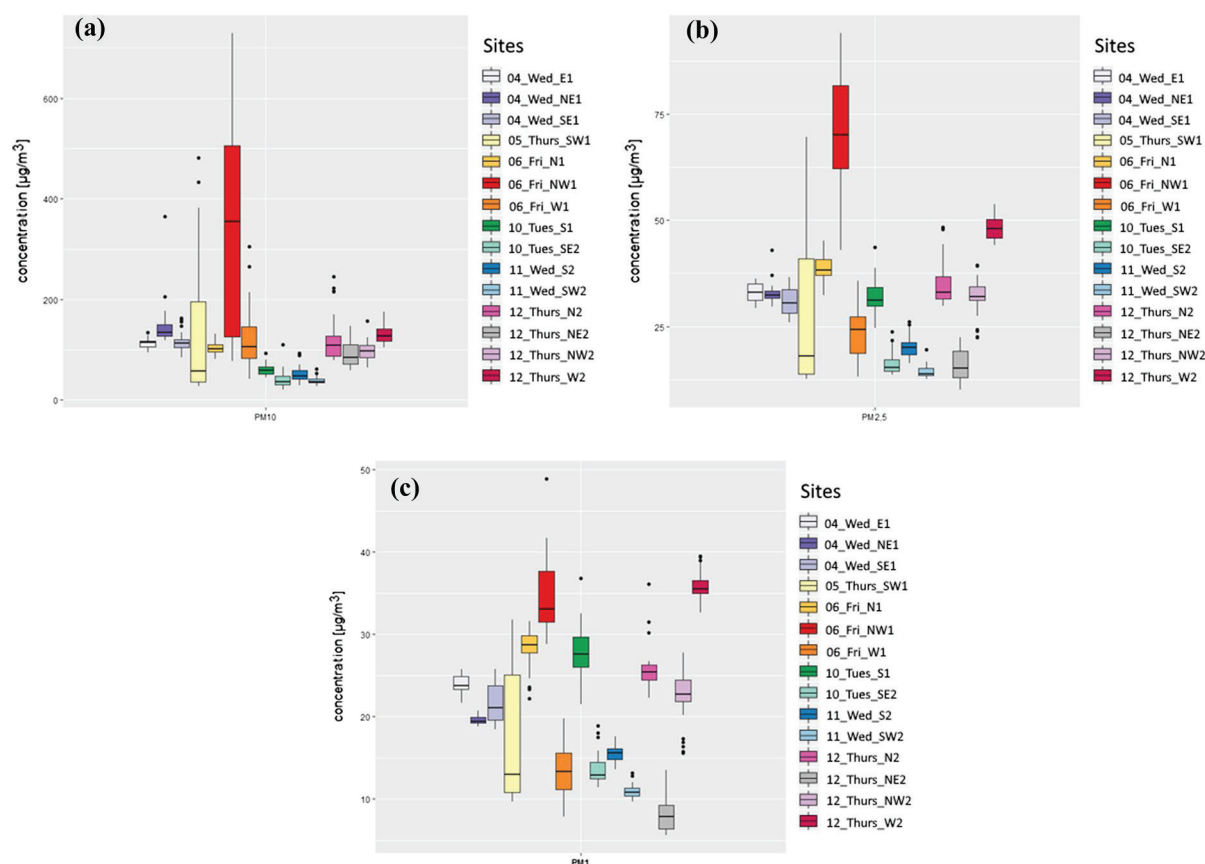
Fig. 5 Boxplot diagrams in µg m^{-3} for the 15 sampling sites: **a** PM$_{10}$; **b** PM$_{2.5}$; and **c** PM$_1$

Particle number distribution

Figure 6 shows that particle number distribution is mostly below 0.5 µm, i.e. correspond to ultra-fine particles. Figure 6a shows particle number distribution sampled between 4 September and 6 September. The sub-micrometric fraction shows similar distributions for all sampling sites, with NE1 and W1 registering the lowest values, in the range between 0.25 µm and 0.70 µm. Particle number of the PM$_1$ fraction fluctuates between 99.5% in W1 to 99.8% in E1 and SE1. The fraction of PM$_{1-2.5}$ shows similar distributions in all sites, with site NW1 being the highest and SE1 the lowest, and in the range between 1.0 µm to 2.0 µm, and the site N1 in the range between 2.0 µm to 2.5 µm. The site N1 located at ~700 m from NW1 and sampled the same day shows the lowest particle number concentration, which evidences the spatial variability of concentration in mass and in

particle number, in sites located at a short distance. The > PM$_{10}$ fraction shows a greater variability in the distributions than the other fractions.

Figure 6b shows particle number distribution of samples taken on 10 September to 12 September 2019. Particle number percentage registered in the sub-micrometric fraction was between 99.4% (at NE2) and 99.9% (at the sites S1, SE2 and N2) of the total, as in the first sampling week. The sub-micrometric fraction shows that the sites with the highest number of particles are the site S1, in the range of 0.25 µm to 0.45 µm, site N2, in the range of 0.45 µm to 0.60 µm, and site W2, in the range 0.60 µm to 1.00 µm. The < 1.1 µm range (i.e. ultra-fine particles) is linked to fossil fuel combustion such as thermoelectric power plant emissions. As mentioned before, a thermoelectric power plant is located ~1.7 km west from the sampling sites. The lowest concentration, between 0.25 µm and 0.60 µm range, was obtained
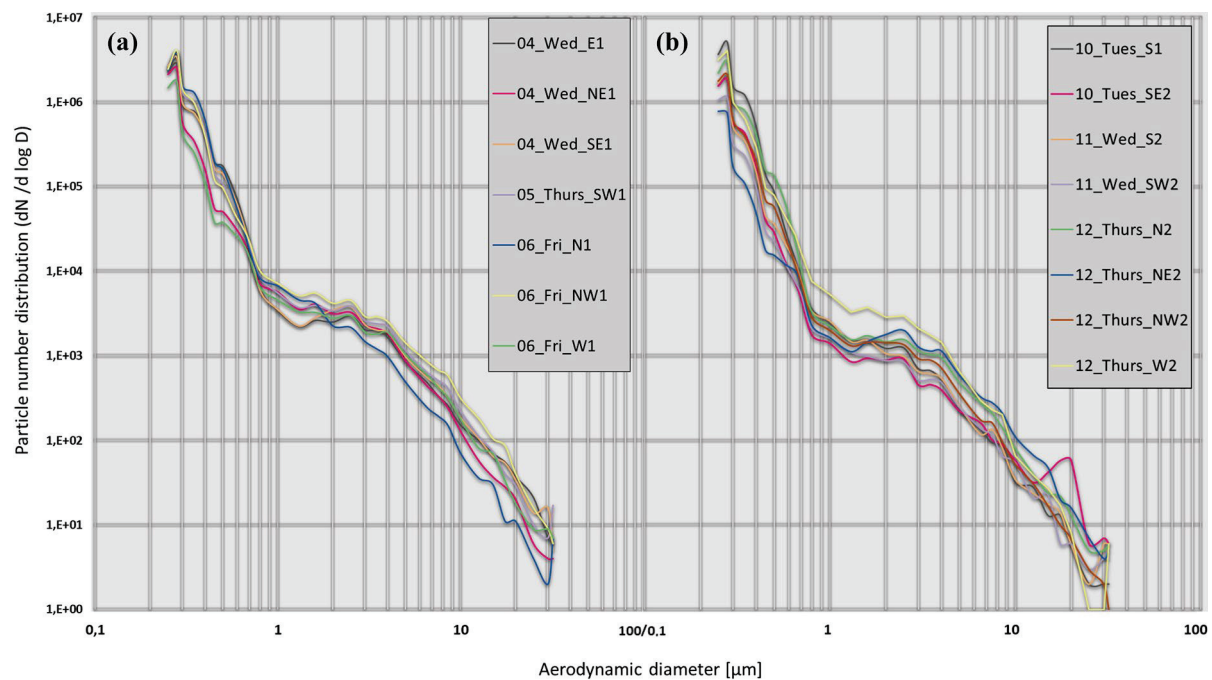
Fig. 6 Particle number distribution (dN/dlogD) at the 15 sampling sites: **a** 4 to 6 September 2019; **b** 10 to 12 September 2019. *X*-axis and *y*-axis are in logarithmic (base 10) scale

at NE2, without observed local sources and with a medium–low level of traffic. The 0.60 μm to 5.00 μm range shows the lowest concentrations at sites SE2 and SW2, where similar distributions were obtained, which can be attributed to vegetate areas proximity. In the $PM_{1–2.5}$ range, the W2 site shows a particle number higher than other sites. In the $PM_{2.5–10}$ range, W2 shows the highest number of particles between 2.5 μm and 6.5 μm. W2 was exceeded by NE2 in the 6.5 μm to 10 μm range.
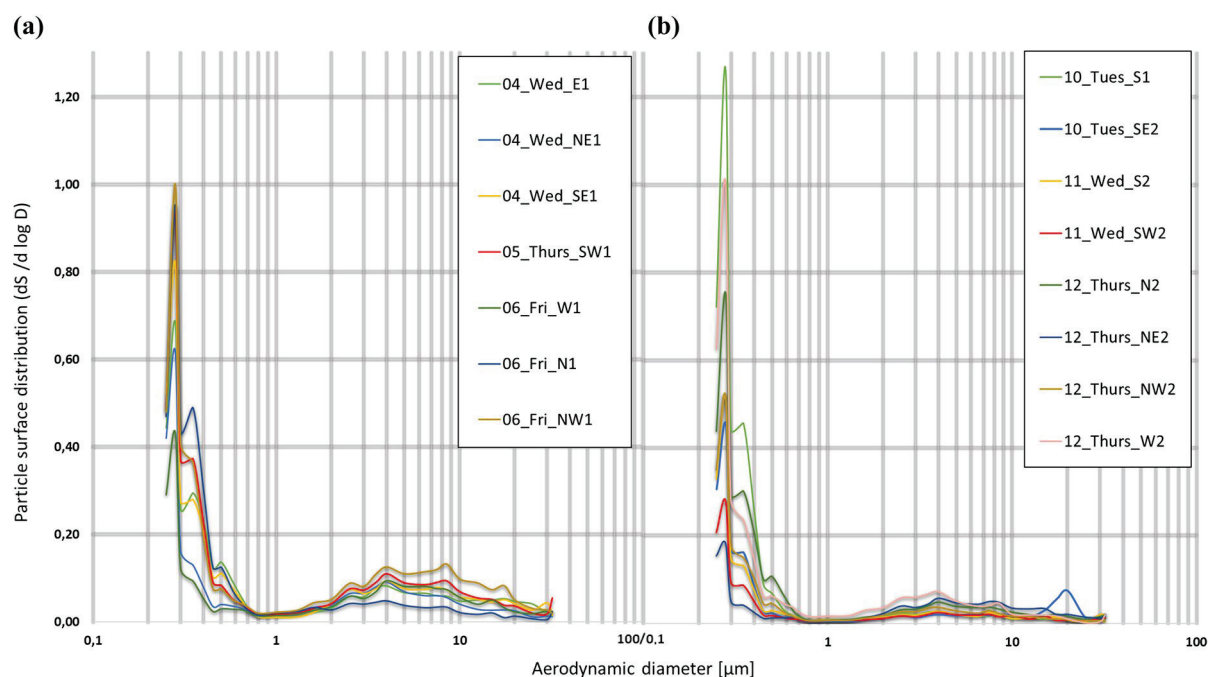
Particle surface distribution

Figure 7 shows particle surface distribution of samples taken between 4 September and 12 September. The figure shows two peaks at almost all sites. The first peak is present at all sites, with particles less than 0.3 μm; the second peak is located between 0.28 μm and 0.4 μm. Figure 7a shows the results for the samples taken on 4 September to 6 September. The largest peak is found at all sites at 0.28 μm; a second peak appears at 0.35 μm. There is high distribution variability in the 0.25 μm to 0.65 μm range followed by a convergence of all distribution curves. In the $PM_{1–2.5}$

range, something similar is found. In the $PM_{2.5–10}$ range, the distributions become different again, which may be due to particle number differences (Fig. 6).

Figure 7b shows particle surface distributions for the second sampling period. The highest surface percentage is found at the sub-micrometric fraction, accumulating between 55.2% (siteW1) and 85.4% (site N1), of the total PM surface. The largest surface area is concentrated in the sub-micrometric fraction, which accumulates between 47.1% (site NE2) and 92.4% (site S1) of the total PM surface, a more extended range than PM collected during the first sampling period. The surface contribution from the larger aerodynamic diameter ranges is smaller than the observed in Fig. 8a.

The surface maximum is reached at 0.28 μm at all the sites. The observed variability in particle surface distribution is attributable to differences in traffic levels. Particle surface distributions converge in the 0.80–1.30 μm range with minimal surface contribution. Subsequently, the $PM_{2.5–10}$ and $PM_{10–32}$ ranges have a lower surface concentration than the first sampling period. The peak observed at SE2 was also registered in particle number distribution (Fig. 6b).

(a)　　　　　　　　　　　　　　　　　　　　　**(b)**

Fig. 7 Particle surface distribution (dN/dlogD) at the 15 sampling sites during: **a** 4 September to 6 September 2019; **b** 10 September to 12 September 2019. X-axis and y-axis are depicted in logarithmic (base 10) scale

Discussion

There is a pharmaceutical industry and a mill located to the NW and W direction from the ORMS-IS (Fuentealba, 2018; Préndez et al., 2007); in addition, the General Cemetery crematorium and La Recoleta Cinerary locate at N and NE from the ORMS-IS, respectively. The above-mentioned industries and services are associated with < 2.5 μm particles emissions (Figs. 1 and 2). The Renca thermoelectric power plant and the industries located in the SW sector of the city (Fuentealba, 2018) can also affect the sampling sites with ultra-fine particles. Previous studies report the presence of Co, Cu, Fe, Na, Sb and Zn in the fine particle size range linked with vehicular emissions (Fuentealba, 2018) in samples collected near the highway Autopista Central. Miler, (2021) in the city of Ljubljana (Slovenia) also found some of those elements coming from vehicle exhaust emissions, brake disc dust and road sediment. Thursday September 5 presented a predominant SE wind direction and lower frequency regimes varying during the day as NW, NE and N (Fig. 3). To note that ultra-fine PM (PM less than 1 μm) can penetrate deeper into the respiratory system (Chen et al., 2016; Shiraiwa et al., 2017), clearly affecting respiratory and cardiovascular systems.

All sampled sites are affected by high, medium or low traffic of personal and public traffic. The highest surface and particle number vales for the site NW1 were found at the PM$_{2.5–10}$ range, which have also the highest PM concentrations.

On the other hand, 11 of the 15 sampling sites are near vegetated areas, including some densely vegetated covers such as San Cristóbal and Blanco hills (located E and NE from the sampling sites) and Los Reyes and Forestal parks (located S and SW from the sampling sites) (Fig. 1). Vegetation contributes to improve air quality due to the capture of PM and the absorption of gases (Escobedo et al., 2011; Gao et al., 2015; Nowak et al., 2013; Préndez et al., 2019). On the > PM10 fraction, a peak was observed at SE2 which coincides with the pollen size range (Ramli et al., 2020). Pollen varies in shape and size (from 10 μm to 100 μm) depending on the species. Two different tree species present at the Metropolitan Park have their pollination period during September–October: *Platanus* x *acerifolia* and *Acer negundo*. The
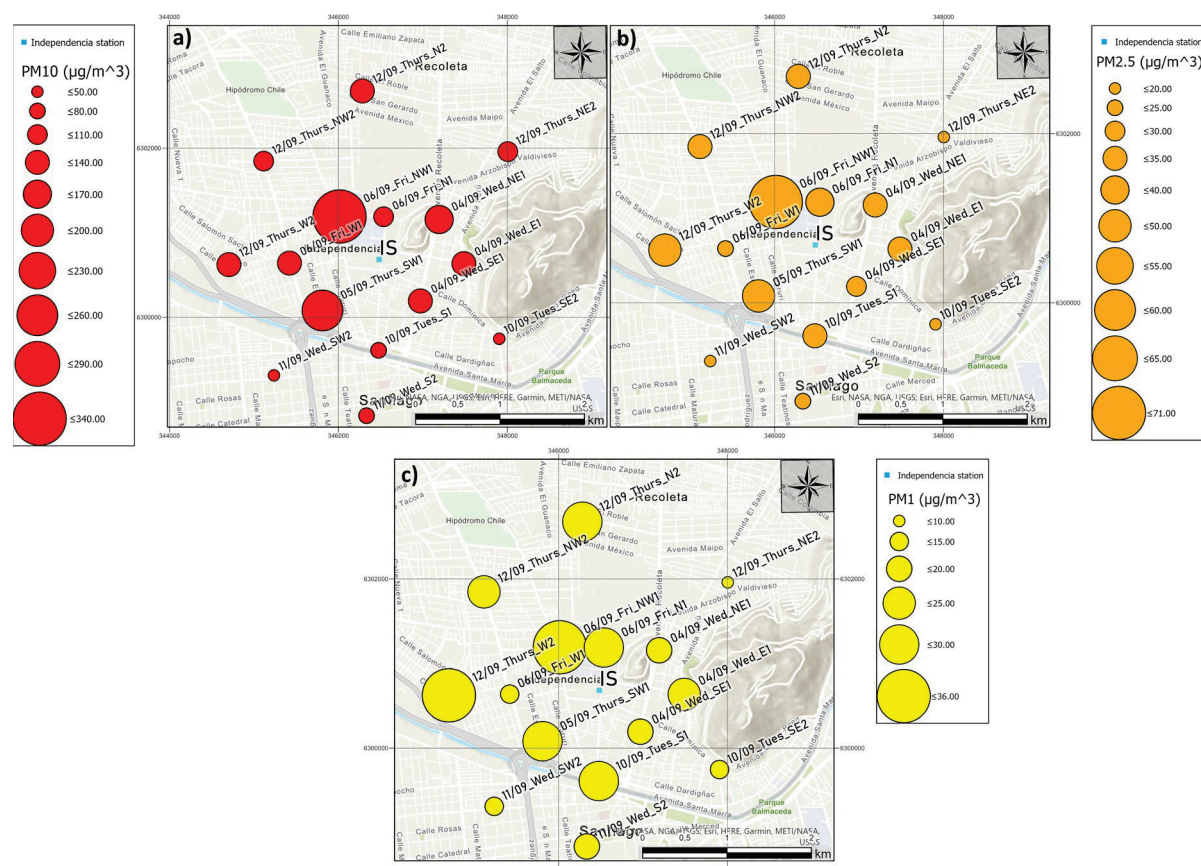
Fig. 8 Spatial analysis of the concentrations of PM sampled in the representative area of the ORMS-IS: **a** PM_{10}; **b** $PM_{2.5}$ and **c** PM_1

Cupressus sempervirens has its pollination period during August–September (PARQUEMET, 2017). In addition to the emission of pollen, site W2 is interesting since it shows the highest number of particles between 2.5 μm and 6.5 μm, and the lowest number of particle surface.

Trees also constitute a natural source of fine PM due to the emission of volatile organic compounds, potential ozone precursors and fine secondary organic compounds (SOA), having a complex chemical composition (Nault et al., 2018; Préndez et al., 2013).

The highest surface percentage of the particle surface distributions is found at the sub-micrometric fraction, which is mostly influenced by anthropic emissions (Gietl et al., 2010; Perrone et al., 2014; Sinha et al., 2011; Zhao & Yu, 2017). However, the percentages are not as high as those observed in the number of particles (99.5% to 99.8%). This is because at the $MP_{2.5-10}$ range, the particles are few in number;

however, they represent a significant contribution to particle surface.

Figure 8 shows the spatial analysis of PM concentrations: a) PM_{10}; b) $PM_{2.5}$ and c) PM_1. Figure 8a shows that the highest concentration of PM_{10} and $PM_{2.5}$ corresponds to site NW1 (on 6 September). High concentrations at this site are probably due to the influence of local sources such as high vehicular traffic, re-suspended dust deposited on the pavement, abrasion of vehicle brakes, tyres and pavement degradation, and building construction (Gietl et al., 2010; Thorpe et al., 2007). In addition, the sampling site is in front of Hospitales subway station that presents a large flow of people during daytime. This site also shows the second highest concentration of PM_1 and a high number of particles of large surface, thus constituting a dangerous site for human health in case of prolonged exposure. However, during the sampling hours, the ORMS-IS station report

concentrations of 74 µg m^{-3} and 23 µg m^{-3} for PM$_{10}$ and PM$_{2.5}$, respectively, 4.6 and 3.0 times lower than the observed values in this work ((339 ± 214) µg m^{-3} and (70 ± 13) µg m^{-3}, respectively). Concentrations of PM$_{10}$ and PM$_{2.5}$ at site SW1 are lower than NW1, with (230 ± 89) µg m^{-3} and (43 ± 8) µg m^{-3}, respectively (Fig. 8b). At the other sites, there are also differences between concentrations of PM$_{10}$ and PM$_{2.5}$. Mean concentrations for 24 h for the daily report by ORMS-IS are 43 µg m^{-3} and 13 µg m^{-3} for PM$_{10}$ and PM$_{2.5}$, respectively (MMA, 2021a, 2021b).

Minimum concentrations of PM$_{10}$, PM$_{2.5}$ and PM$_1$ occurred on 11 September at SW2, with (39 ± 7) µg m^{-3}, (14 ± 2) µg m^{-3} and (11 ± 1) µg m^{-3}. This day registered a mild rain (Figure SI-2), with rainfall often contributing to decrease atmospheric PM concentration (Nowak et al., 2013; Préndez et al, 2014). In the case of ORMS-IS station, SINCA reports concentrations of 23 µg m^{-3} and 3 µg m^{-3} for PM$_{10}$ and PM$_{2.5}$, respectively, during the sampled hours of this work, but does not report accumulative values for 24 h (MMA, 2021a).

PM$_1$ concentrations show a completely different spatial distribution than PM$_{10}$ and PM$_{2.5}$. Sites SW1 and W2 show the highest PM concentrations. It is interesting to note that the site W2 increases their mass relative concentration in the sense inverse to the diameter of the particles (Fig. 8c).

Currently in Chile, there are no official standards for the PM sub-micrometric fraction. The lowest PM$_1$ concentrations were obtained at the sites SW2, S2, SE2, and NE2, sampled at the ORMS-IS area boundary. The W2 site showed the highest concentration of PM$_1$ probably due to its closeness to Autopista Central and Renca thermoelectric power plant, as discussed by Wang et al. (2005) in relation to combustion of fossil fuels.

In the sites located within 1 km from the ORMS-IS, the lowest PM$_1$ concentration and particle number was recorded at W1 (at 0.28 µm). This site presents medium/low traffic, without vegetated areas close by, but potentially affected by three gas stations. Using a similar optical spectrophotometer as the one used in this study, Dahari et al., 2021 observed a peak of the number of particles in the submicron range with percentages of the order of more than 95% and attributed these findings mainly to vehicular traffic. Site S1 shows mass concentrations higher than the PM$_1$ average (between 17.7% and 58.7%) and the

highest number of particles in the range of 0.25 µm to 0.45 µm. This site is the closest to local sources of street cooking that use different combustion types, such as gas stoves for frying or open charcoal grills. The < 1.1 µm range (i.e. ultra-fine particles) is linked to combustion of fossil fuels (Rajput et al., 2016; Wang et al., 2005). In addition, Buonanno et al. (2009) reported the highest percentage of particles from such outdoor cooking coming from activities in the (0.1–1.0) µm range, followed by PM within the (1.0–2.5) µm range. The precariousness of the facilities for street cooking leads to poor combustion; therefore, for this reason, additional research in this topic is necessary to assess the contributing of this PM source.

Independencia municipality, as all the peri-central areas, has increased its urban functionality, density and mobility, during recent years, and it is expected that this trend would continue in the near future. Hospitals, in addition to the largest open market of the city (La Vega), large cemeteries, a large subway station, and heavy traffic roads for private and public transportation have not been the object of systematic environmental planning and management. Vegetation cover is poor and not distributed according to their ecological services. The eventual arrival of clean air masses from nearby hills and parks is constrained by the roughness of an increasing number and density of high-rise buildings. It is necessary for Santiago and other large Latin American cities to incorporate air pollution spatial and temporal detailed information in their sustainable urban development. The presence of such a large number of sources without counterbalancing actions contributes air pollution and increases the population's risk of contracting respiratory and/or cardiovascular diseases.

Conclusions

New characteristics of aerosol not measured at present by the official air quality monitoring network were quantified within the ORMS-IS area. All 15-sites show the highest values of particle number distributions in the range of ultra-fine particles. Surface distributions at all sites showed that particle size was mostly below 0.4 µm (i.e. nanometric particles), with high potential to absorb other pollutants.

Differences in PM mass concentration, particle number and particle surface distribution were observed within the representative area of the ORMS-IS. PM at the area was most likely due to local sources around the microenvironment, e.g. vehicular traffic, building construction, street cooking and pollen emissions. PM hot spots can be individualized within the studied area, with important implications for human health, including seasonal allergies.

PM_{10} data provided by the ORMS-IS represent well the sites near the station. On the contrary, $PM_{2.5}$ and PM_1 are not well represented by the ORMS-IS.

The importance of ultra-fine PM ($<PM1$) and other characteristics of the aerosol such as particle surface and particle number distribution evidence the different quality of air within the monitored area and potential effects on population health. This heterogeneity is the result of local sources, in addition to specific urban conditions and/or the lack of management policies.

The complementary setting of a monitoring network based on instruments assessing the different properties of the aerosol could contribute to improve air pollution policy making at Santiago city.

Author contributions All authors contributed to the study conception and design. Material preparation, data collection and analysis were performed by PN and MP. The first draft of the manuscript was written by PN, MP and HR, and all authors commented on previous versions of the manuscript. All authors read and approved the final manuscript.

Data availability See web page https://figshare.com/articles/dataset/_/16441707

Declarations

Conflict of interest The authors declare that they have no known competing financial interests or personal relationships that could have appeared to influence the work reported in this paper.

Consent for publication The authors also declare that the work sent for publication does not include material from third parties that are subject to copyright (figures, tables, photos or others similar).

Ethical approval The corresponding author Margarita Préndez, and on its behalf the rest of the authors, declares that the individualized article above represents results of original research, that is has not been published nor is being considered for publication in another journal, and that it complies with international ethical standards of intellectual property and authorship.

References

Bind, M. A., Baccarelli, A., Zanobetti, A., Tarantini, L., Suh, H., Vokonas, P., & Schwartz, J. (2012). Air pollution and markers of coagulation, inflammation, and endothelial function: Associations and Epigene-environment interactions in an Elderly Cohort. *Epidemiology, 23*(2), 332–340. https://doi.org/10.1097/ede.0b013e31824523f0

Buccolieri, R., Sandberg, M., & Di Sabatino, S. (2010). City breathability and its link to pollutant concentration distribution within urban-like geometries. *Atmospheric Environment, 44*(15), 1894–1903. https://doi.org/10.1016/j.atmosenv.2010.02.022

Buonanno, G., Morawska, L., & Stabile, L. (2009). Particle emission factors during cooking activities. *Atmospheric Environment, 43*(20), 3235–3242. https://doi.org/10.1016/j.atmosenv.2009.03.044

Cassee, F. R., Héroux, M. E., Gerlofs-Nijland, M. E., & Kelly, F. J. (2013). Particulate matter beyond mass: Recent health evidence on the role of fractions, chemical constituents and sources of emission. *Inhalation Toxicology, 25*(14), 802–812. https://doi.org/10.3109/08958378.2013.850127

Chen, R., Hu, B., Liu, Y., Xu, J., Yang, G., Xu, D., & Chen, C. (2016). Beyond PM2. 5: The role of ultrafine particles on adverse health effects of air pollution. *Biochimica Et Biophysica Acta (BBA) General Subjects., 1860*, 2844–2855.

Dahari, N., Muda, K., Latif, M. T., Dominick, D., Hussein, N., & Khan, M. F. (2021). Seasonal variations of particle number concentration and its relationship with PM2.5 mass concentration in industrial residential airshed. *Environmental Geochemistry and Health.* https://doi.org/10.1007/s10653-021-01099-3

Dinoi, A., Donato, A., Belosi, F., Conte, M., & Contini, D. (2017). Comparison of atmospheric particle concentration measurements using different optical detectors:

Potentiality and limits for air quality applications. *Measurement, 106*, 274–282. https://doi.org/10.1016/j.measurement.2016.02.019

DMC. (2021). Reporte Anual de la Evolución del Clima en Chile, 2020. *Oficina de Cambio Climático, Sección de Climatología, Dirección Meteorológica de Chile (DMC). Dirección General de Aeronáutica Civil (DGAC)*. Mayo, 2021. Retrieved May 1, 2020. https://cambioclimatico.mma.gob.cl/wp-content/uploads/2021/06/ReporteClimatico2020-edmay2021.pdf

Escobedo, F. J., Kroeger, T., & Wagner, J. E. (2011). Urban forests and pollution mitigation: Analyzing ecosystem services and disservices. *Environmental Pollution, 159*(8–9), 2078–2087. https://doi.org/10.1016/j.envpol.2011.01.010

Forlivesi, S., Turcato, G., Zivelonghi, C., Zannoni, M., Ricci, G., Cervellin, G., Lippi, G., Bovi, P., Bonetti, B., & Cappellari, M. (2018). Association of short-and medium-term particulate matter exposure with risk of mortality after spontaneous intracerebral hemorrhage. *Journal of Stroke and Cerebrovascular Diseases, 27*(9), 2519–2523. https://doi.org/10.1016/j.jstrokecerebrovasdis.2018.05.007

Fuentealba, R. (2018). Caracterización y estimación de fuentes del polvo urbano y material particulado del sector norte de Santiago mediante métodos no destructivos de análisis elemental. Tesis para optar al grado de Magíster en Química. Universidad de Chile. https://www.postgradoquimica.cl/egresados-postgrado/page/8/.

Galvão, E., Santos, J., Lima, A., Reis, N., Orlando, M., & Stuetz, R. (2018). Trends in analytical techniques applied to particulate matter characterization: A critical review of fundaments and applications. *Chemosphere, 199*, 546–568. https://doi.org/10.1016/j.chemosphere.2018.02.034

Gao, G., Sun, F., Thao, N. T. T., Lun, X., & Yu, X. (2015). Different concentrations of TSP, PM10, PM2.5, and PM1 of several urban forest types in different seasons. *Polish Journal of Environmental Studies, 24*(6), 2387–2395. https://doi.org/10.15244/pjoes/59501

Gietl, J. K., Lawrence, R., Thorpe, A. J., & Harrison, R. M. (2010). Identification of brake wear particles and derivation of a quantitative tracer for brake dust at a major road. *Atmospheric Environment, 44*(2), 141–146. https://doi.org/10.1016/j.atmosenv.2009.10.016

Grimm, H., & Eatough, D. J. (2009). Aerosol Measurement: The use of optical light scattering for the determination of particulate size distribution, and particulate mass, including the semi-volatile fraction. *Journal of the Air and Waste Management Association, 59*, 101–107. https://doi.org/10.3155/1047-3289.59.1.101

Guo, J., Zhai, Z., Wang, L., Wang, Z., Wu, J., Zhang, B., & Zhang, J. (2017). Dynamic and thermodynamic mechanisms of TFA adsorption by particulate matter. *Environmental Pollution, 225*, 175–183. https://doi.org/10.1016/j.envpol.2017.03.049

HEI (2019). State of Global Air (2019): A Special Report on Global Exposure to Air Pollution. *Health Effects Institute (HEI)*. Boston, MA: ISSN 2578–6873 Retrieved May 1, 2020, from https://www.stateofglobalair.org/sites/default/files/soga_2019_report.pdf.

Hofman, J., Stokkaer, I., Snauwaert, L., & Samson, R. (2013). Spatial distribution assessment of particulate matter in an urban street canyon using biomagnetic leaf monitoring of tree crown deposited particles. *Environmental Pollution, 183*, 123–132. https://doi.org/10.1016/j.envpol.2012.09.015

Holstius, D. M., Pillarisetti, A., Smith, K. R., & Seto, E. (2014). Field calibrations of a low-cost aerosol sensor at a regulatory monitoring site in California. *Atmospheric Measurement Techniques, 7*(4), 1121–2113. https://doi.org/10.5194/amt-7-1121-2014

INE. (2022). Demografía y vitales. *Instituto Nacional de Estadísticas (INE)*. Retrieved May 6, 2022, from https://www.ine.cl/estadisticas/sociales/demografia-y-vitales.

Jorquera, H. (2020). Ambient particulate matter in Santiago, Chile: 1989–2018: A tale of two size fractions. *Journal of Environmental Management, 258*, 110035. https://doi.org/10.1016/j.jenvman.2019.110035

Karner, A. A., Eisinger, D. S., & Niemeier, D. A. (2010). Near-Roadway Air Quality: Synthesizing the findings from real-world data. *Environmental Science & Technology, 44*(14), 5334–5344. https://doi.org/10.1021/es100008x

Kelly, K. E., Whitaker, J., Petty, A., Widmer, C., Dybwad, A., Sleeth, D., Martin, R., & Butterfield, A. (2017). Ambient and laboratory evaluation of a low-cost particulate matter sensor. *Environmental Pollution, 221*, 491–500. https://doi.org/10.1016/j.envpol.2016.12.039

Kumar, P., Morawska, L., Martani, C., Biskos, G., Neophytou, M., Di Sabatino, S., Bell, M., Norford, L., & Britter, R. (2015). The rise of low-cost sensing for managing air pollution in cities. *Environment International, 75*, 199–205. https://doi.org/10.1016/j.envint.2014.11.019

Kuuluvainen, H., Rönkkö, T., Järvinen, A., Saari, S., Karjalainen, P., Lähde, T., Pirjola, L., Nieli, J., Hillamo, R., & Keskinen, J. (2016). Lung deposited surface area size distributions of particulate matter in different urban areas. *Atmospheric Environment, 136*, 105–113. https://doi.org/10.1016/j.atmosenv.2016.04.019

Leoni, C., Pokorná, P., Hovorka, J., Masiol, M., Topinka, J., Zhao, Y., Křůmal, K., Cliff, S., Mikuška, P., & Hopke, P. K. (2018). Source apportionment of aerosol particles at a European air pollution hot spot using particle number size distributions and chemical composition. *Environmental Pollution, 234*, 145–154. https://doi.org/10.1016/j.envpol.2017.10.097

Li, Y. R., Feng, L. T., Chen, B. Y., Kim, H., Yi, S. M., Guo, Y. L., & Wu, C. F. (2016). Association of urban particle numbers and sources with lung function among children with asthma or allergies. *Science of the Total Environment, 542*, 841–844. https://doi.org/10.1016/j.scitotenv.2015.10.098

Long, C. M., Nascarella, M. A., & Valberg, P. A. (2013). Carbon black vs. black carbon and other airborne materials containing elemental carbon: Physical and chemical distinctions. *Environmental Pollution, 181*, 271–286. https://doi.org/10.1016/j.envpol.2013.06.009

Mendes, F. H., Romero, H., da Silva, F., & Filho, D. (2020). Cambio climático adverso provocado por la urbanización sin planificación ambiental en Santiago de Chile. *Revista De Geografía Norte Grande, 77*, 191–210. https://doi.org/10.4067/S0718-34022020000300191

Miler, M. (2021). Airborne particles in city bus: Concentrations, sources and simulated pulmonary solubility.

Environmental Geochemistry and Health, 43, 2757–2780. https://doi.org/10.1007/s10653-020-00770-5

MINSAL. (1998). Resolución N° 11481. Clasifica Estaciones de Monitoreo de Material Particulado Respirable MP10. *Ministerio de Salud (MINSAL)*; Servicio de Salud del Ambiente Región Metropolitana. Enacted: 10–06–1998. Published: 18–06–1998. http://bcn.cl/31sn1.

MMA. (2017). Resolución 744 Exenta. Establece Criterios para Calificar Estaciones de Monitoreo de Material Particulado Respirable (MP10) como de Representatividad Poblacional. *Ministerio Del Medio Ambiente (MMA)*; Superintendencia del Medio Ambiente (SMA). Enacted: 11–07–2017. Published: 19–07–2017. http://bcn.cl/2o9bi.

MMA. (2019). Estación Independencia: Parámetros Meteorológicos. Sistema de Información Nacional de Calidad del Aire (SINCA). *Ministerio de Medio Ambiente (MMA)*. Retrieved September 30, 2019, from https://sinca.mma.gob.cl/index.php/estacion/index/id/272.

MMA. (2021a). Sistema de Información Nacional de Calidad del Aire (SINCA). Ministerio de Medio Ambiente (MMA). Retrieved May 3, 2021a, from https://sinca.mma.gob.cl/index.php/.

MMA. (2021a). Estación Independencia: Parámetros contaminantes. Sistema de Información Nacional de Calidad del Aire (SINCA). *Ministerio de Medio Ambiente (MMA)*. Retrieved June 12, 2021b, from https://sinca.mma.gob.cl/index.php/estacion/index/id/272.

Nault, B. A., Campuzano-Jost, P., Day, D. A., Schroder, J. C., Anderson, B., Beyersdorf, A. J., Blake, D. R., Brune, W. H., Choi, Y., Corr, C. A., de Gouw, J. A., Dibb, J., DiGangi, J. P., Diskin, G. S., Fried, A., Huey, L. G., Kim, M. J., Knote, C. J., Lamb, K. D., … Jimenez, J. L. (2018). Secondary organic aerosol production from local emissions dominates the organic aerosol budget over Seoul, South Korea, during KORUS-AQ. *Atmospheric Chemistry and Physics, 18*(24), 17769–17800. https://doi.org/10.5194/acp-18-17769-2018

Nowak, D. J., Hirabayashi, S., Bodine, A., & Hoehn, R. (2013). Modeled PM2.5 removal by trees in ten U.S. cities and associated health effects. *Environmental Pollution, 178*, 395–402. https://doi.org/10.1016/j.envpol.2013.03.050

Ntziachristos, L., Polidori, A., Phuleria, H., Geller, M. D., & Sioutas, C. (2007). Application of a diffusion charger for the measurement of particle surface concentration in different environments. *Aerosol Science and Technology, 41*(6), 571–580. https://doi.org/10.1080/02786820701272020

PARQUEMET. (2017). Guía de reconocimiento de árboles del Parque Metropolitano de Santiago: "Los árboles del Parque". *Parque Metropolitano de Santiago (PARQUEMET)*. Retrieved June 12, 2020, from https://www.parquemet.cl/wp-content/uploads/2018/05/libro-arboles_issuu3.pdf.

Perrone, M. R., Dinoi, A., Becagli, S., & Udisti, R. (2014). Chemical composition of PM1 and PM2.5 at a suburban site in southern Italy. *International Journal of Environmental Analytical Chemistry, 94*(2), 127–150. https://doi.org/10.1080/03067319.2013.791978

Préndez, M., Corvalán, R. M., & Cisternas, M. (2007). Estudio preliminar del material particulado de fuentes estacionarias: Aplicación al sistema de compensación de emisiones en la Región Metropolitana Chile. *Información Tecnológica, 18*(2), 93–103. https://doi.org/10.4067/S0718-07642007000200015

Préndez, M., Carvajal, V., Corada, K., Morales, J., Alarcón, F., & Peralta, H. (2013). Biogenic volatile organic compounds from the urban forest of the Metropolitan Region, Chile. *Environmental Pollution, 183*, 143–150. https://doi.org/10.1016/j.envpol.2013.04.003

Préndez, M., López, R., & Carrillo, E. (2014). Physical and chemical components of Cuba's rain: Effects on air quality. *International Journal of Atmospheric Sciences, 2014*(680735), 8.

Préndez, M., Araya, M., Criollo, C., Egas, C., Farías, I., Fuentealba, R., & González, E. (2019). Urban trees and their relationship with air pollution by particulate matter and ozone in Santiago, Chile. In C. Henríquez & H. Romero (Eds.), *Urban Climates in Latin America*. Springer. https://doi.org/10.1007/978-3-319-97013-4_8

Préndez, M., Alvarado, G., & Serey, I. (2011). Some Guidelines to Improve the Air Quality Management of Santiago, Chile. In N. Mazzeo (Ed.), *Air Quality Monitoring*. IntechOpen: Assessment and Management. https://doi.org/10.5772/19638

Rajput, P., Mandaria, A., Kachawa, L., Singh, D. K., Singh, A. K., & Gupta, T. (2016). Chemical characterisation and source apportionment of PM1 during massive loading at an urban location in Indo-Gangetic Plain: Impact of local sources and long-range transport. *Tellus B: Chemical and Physical Meteorology, 68*(1), 30659. https://doi.org/10.3402/tellusb.v68.30659

Ramli, N. A., Md Yusof, N. F. F., Shith, S., & Suroto, A. (2020). Chemical and biological compositions associated with ambient respirable particulate matter: A review. *Water Air Soil Pollution, 231*(3), 1–14. https://doi.org/10.1007/s11270-020-04490-5

Romero, H., Irarrázaval, F., Opazo, D., Salgado, M., & Smith, P. (2010). Climas urbanos y contaminación atmosférica en Santiago de Chile. *EURE (santiago), 36*(109), 35–62. https://doi.org/10.4067/S0250-71612010000300002

Sarricolea, P., Smith, P., Romero-Aravena, H., Serrano-Notivoli, R., Fuentealba, M., & Meseguer-Ruiz, O. (2022). Socioeconomic inequalities and the surface heat island distribution in Santiago. *Chile. Science of the Total Environment, 832*, 155152. https://doi.org/10.1016/j.scitotenv.2022.155152

Setti, L., Passarini, F., De Gennaro, G., Barbieri, P., Perrone, M. G., Piazzalunga, A., Borelli, M., Palmisani, J., Di Gilio, A., Piscitelli, P., & Miani, A. (2020). The potential role of particulate matter in the spreading of COVID-19 in northern Italy: First evidence-based research hypotheses. *MedRxiv*. https://doi.org/10.1101/2020.04.11.20061713

Shiraiwa, M., Ueda, K., Pozzer, A., Lammel, G., Kampf, C. J., Fushimi, A., Shinichi, E., Arangio, A. M., Fröhlich-Nowoisky, J., Fujitani, Y., Furuyama, A., Lakey, P., Lelieveld, J., Lucas, K., Morino, Y., Pöschl, U., Takahama, S., Takami, A., Tong, H., … Sato, K. (2017). Aerosol health effects from molecular to global scales. *Environmental Science & Technology, 51*(23), 13545–13567. https://doi.org/10.1021/acs.est.7b04417

Sinha, P. R., Manchanda, R. K., Kaskaoutis, D. G., Sreenivasan, S., Moorthy, K. K., & Babu, S. S. (2011).

Spatial heterogeneities in aerosol size distribution over Bay of Bengal during winter-ICARB experiment. *Atmospheric Environment, 45*(27), 4695–4706. https://doi.org/10.1016/j.atmosenv.2011.04.085

Thorpe, A. J., Harrison, R. M., Boulter, P. G., & McCrae, I. S. (2007). Estimation of particle resuspension source strength on a major London Road. *Atmospheric Environment, 41*(37), 8007–8020. https://doi.org/10.1016/j.atmosenv.2007.07.006

Toro, R., Morales, R., Canales, M., González-Rojas, C., & Leiva, M. (2014). Inhaled and inspired particulates in Metropolitan Santiago Chile exceed air quality standards. *Building and Environment, 79*, 115–123. https://doi.org/10.1016/j.buildenv.2014.05.004

Tsai, D., Riediker, M., Berchet, A., Paccaud, F., Waeber, G., Vollenweider, P., & Bochud, M. (2019). Effects of short- and long-term exposures to particulate matter on inflammatory marker levels in the general population. *Environmental Science and Pollution Research, 26*(19), 19697–19704. https://doi.org/10.1007/s11356-019-05194-y

TSI. (2012). Aerosol statistics lognormal distributions and dN/dlogDp. Application Note PR-001 Rev B. *TSI Incorporated*, U.S.A. Retrieved September 19, 2019, from https://tsi.com/getmedia/1621329b-f410-4dce-992b-e21e1584481a/PR-001-RevA_Aerosol-Statistics-AppNote?ext=.pdf.

USEPA. (2004). Air quality criteria for particulate matter (Final Report, 2004), U.S. Environmental Protection Agency, Washington, DC, EPA 600/P-99/002aF-bF. Retrieved June 24, 2019, from https://cfpub.epa.gov/si/si_public_record_report.cfm?Lab=NCEA&dirEntryId=87903.

Wang, X., Sato, T., Xing, B., Tamamura, S., & Tao, S. (2005). Source identification, size distribution and indicator screening of airborne trace metals in Kanazawa Japan. *Journal of Aerosol Science, 36*(2), 197–210. https://doi.org/10.1016/j.jaerosci.2004.08.005

Wang, Y., Li, J., Jing, H., Zhang, Q., Jiang, J., & Biswas, P. (2015). Laboratory evaluation and calibration of three low-cost particle sensors for particulate matter measurement. *Aerosol Science and Technology, 49*(11), 1063–1077. https://doi.org/10.1080/02786826.2015.1100710

WHO. (2022). Urban health. *World Health Organization (WHO)*. Retrieved May 1, 2022, from https://www.who.int/news-room/fact-sheets/detail/urban-health.

Zhao, S., & Yu, Y. (2017). Effect of short-term regional traffic restriction on urban submicron particulate pollution. *Journal of Environmental Sciences, 55*, 86–99. https://doi.org/10.1016/j.jes.2016.06.023

Zikova, N., Hopke, P. K., & Ferro, A. R. (2017). Evaluation of new low-cost particle monitors for PM2.5 concentrations measurements. *Journal of Aerosol Science, 105*, 24–34. https://doi.org/10.1016/j.jaerosci.2016.11.010

Zoran, M. A., Savastru, R. S., Savastru, D. M., & Tautan, M. N. (2020). Assessing the relationship between surface levels of PM2.5 And PM10 particulate matter impact on COVID-19 in Milan Italy. *Science of the Total Environment, 738*, 139825.